



Original Paper

Spatial Differentiation Characteristics of Groundwater Stress Index and its Relation to Land Use and Subsidence in the Varamin Plain, Iran

Maryam Nayyeri,¹ Seyed Abbas Hosseini ^{1,3} Saman Javadi,² and Ahmad Sharafati¹

Received 27 April 2020; accepted 22 September 2020
Published online: 10 October 2020

Distributed modeling provides for mapping of spatial and temporal patterns of highly stressed regions, and it offers local solutions to reduce stress in aquifers. In this study, the groundwater stress index (GWSI) is evaluated based on the groundwater footprint index over the Varamin aquifer in Iran. Using ArcGIS software, all necessary layers were produced and then input into the Groundwater Modeling System software to evaluate GWSI. The results show that distributed modeling offers a more accurate assessment of GWSI than water budget analysis. The minimum and maximum values of the GWSI calculated by the distributed model are 2.4 and 1.4 times, respectively, higher than those values obtained in previous studies. Besides, a significant agreement was observed between highly stressed areas and agricultural land use. Furthermore, the results obtained from comparison between stress pattern and land subsidence indicated that only 10% of the area under subsidence was caused by groundwater stress. Applying appropriate scenarios in the future can be useful to reduce water stress and its increasing trend.

KEY WORDS: Groundwater footprint index, Groundwater stress index, Distributed modeling, Land use, Land subsidence.

INTRODUCTION

Freshwater resources include less than 1% of total water available on the planet (WWAP 2009), among which groundwater resources are the main water supply for agriculture and drinking in arid and semiarid regions (Mahmoudi et al. 2017). Therefore, conservation and management of groundwater resources in these regions are very important for governments. Drought conditions, remarkable demand for freshwater, and lack of water availability

during dry seasons are the main reasons of significant groundwater withdrawal in arid and semiarid regions (Das et al. 2018). Information about magnitude of groundwater withdrawals and precise determination of location-based groundwater potential are useful in understanding, managing, and simulating groundwater systems (Das et al. 2018; Das 2019). In particular, the distinction of groundwater potential zones and significant withdrawals areas can help managers and decision-makers to manage aquifers and reduce groundwater stress in arid and semiarid regions (Das et al. 2017, 2018).

The over-exploitation of valuable groundwater resources has lowered the water table depth in recent years, resulting in limitation of the sustainable abstraction of these resources. Among the crucial negative consequences of massive groundwater

¹Department of Civil Engineering, Science and Research Branch, Islamic Azad University, Tehran, Iran.

²Department of Irrigation and Drainage Engineering, College of Abouraihan, University of Tehran, Tehran, Iran.

³To whom correspondence should be addressed; e-mail: abbas_hoseyni@srbiau.ac.ir

abstraction, in addition to decreasing water table depth, are increasing water salinity, lowering water quality, reducing abstraction of deep and semi-deep wells, and severe land subsidence (Al-Naeem 2014). Poor groundwater management causes land subsidence because of soil compression due to groundwater depletion (Pacheco et al. 2006). Groundwater over-exploitation can lead to an increase in probability of land subsidence occurrence (Minderhoud et al. 2018). Several researchers have focused on land subsidence caused by groundwater withdrawal, the main factors controlling the subsidence process, and its basic principles and equations (Gambolati and Teatini 2015; Goode 2016).

In previous studies, several indices have been proposed to evaluate sustainability, vulnerability, and groundwater stress. One of the most widely used indices has been suggested by Gleeson et al. (2012); it is the ratio of rate of total groundwater abstraction to rate of natural recharge and amount of water required to support ecosystems. This groundwater footprint (GWF) introduced by Gleeson et al. (2012) is a scaled image of a basin or watershed outline, the size of which is proportional to the ratio of total withdrawal to available groundwater resource for the basin. The GWF can be used efficiently to visualize the basin-scale magnitudes of groundwater withdrawals from wells.

Dumont et al. (2013) evaluated the water footprint index in the Guadalquivir basin, emphasizing the groundwater. They concentrated on green and blue water footprints and their combination with environmental water requirements. Esnault et al. (2014) studied the relationships between groundwater consumption and stress in some agricultural products using the GWF in the central valley and high plains aquifer systems in the USA. They employed a novel method to find GWF of main crops in aquifers. Kourgialas et al. (2018) applied the approach introduced by Gleeson et al. (2012) to calculate a novel groundwater footprint index (GWFI) for aquifers in Crete Island of Greece. Their methodology focused on both quality and quantity of groundwater systems. Pérez et al. (2019) determined the GWFI for six Colombian aquifers based on several scenarios to improve the consumption of these aquifers. In their calculations, the groundwater parameter related to environmental flow requirements was intentionally ignored, due to the lack of perennial surface water data. Table 1 represents a summary of previous studies on GWF

and their comparison to determine essential parameters for the present study.

As shown in Table 1, previous studies on GWF have focused on a regional scale or some large aquifers referring to water budget methods or conceptual global hydrological models, such as PCR or other semi-distributed models (Gleeson et al. 2013; Esnault et al. 2014; Kourgialas et al. 2018; Pérez et al. 2019). However, limited studies have focused on local aquifers and on using distributed models for small basins (Pérez et al. 2019). Using distributed models, considering the amount of inflow and outflow in every cell provides the possibility of local groundwater stress estimation. In measuring groundwater stress in small aquifers, unlike conceptual global hydrological models, distributed models evaluate applicable approaches for groundwater stress reduction and proper groundwater management by precise estimation of the GWFI. Moreover, generalization of stress in large scales for one aquifer causes an error in decision-making problems.

This paper aims to demonstrate (a) the effectiveness of spatial water stress determination in the Varamin aquifer and (b) the correlation among land use, land subsidence, and stress. This study helps to identify precisely the parts of an aquifer under critical conditions to provide local solutions in groundwater resource management. Quantitative assessment of groundwater in the Varamin aquifer is important because it supplies large amounts of agricultural and drinking water. One of the consequences of long-term and unsystematic abstraction of groundwater is the reduction in water table in the plains, which causes land subsidence. By estimating the groundwater stress index (GWSI), suggestions can be provided for sustainable use of groundwater in critical areas. In addition, the relationships between groundwater stress and subsidence ratio all over the aquifer can be studied considering land subsidence of a plain. The results of this study can be used for aquifers in most arid and semiarid regions in the world with similar geological conditions.

MATERIALS AND METHODS

Study Area

The study area includes the Varamin aquifer located on the southern slope of the Alborz Mountains in the central region of Iran, near the Varamin

Table 1. Review of most cited and recent articles in groundwater footprint

Researchers/ year	Studied area	GWSI main parameters calculation in different articles			Consideration
		C	R	E	
Gleeson et al. (2012)	Pakistan, India, and north-south of Saudi Arabia, and some regions in Iran, Mexico, USA, Egypt, Hungary, Australia, Romania, Mexico, China, Tunisia and Libya and Algeria	(IGRAC)	Global hydrological model PCR-GLOBWB	PCR-GLOBWB	1—Approximate estimation of abstraction parameter (<i>C</i>); 2—Using a conceptual global hydraulic model to estimate recharge (<i>R</i>); 3—Approximate estimation of environmental water requirements (<i>E</i>)
Gleeson et al. (2013)	The USA and India	(CGWB) and (USGS)	Global model	Global model	1—Using large-scale models to estimate (<i>R</i>) and (<i>C</i>) 2—Approximate estimation of (<i>E</i>) and calculated as a fraction of recharge
Kourgialas et al. (2018)	11 Aquifer of Crete Greece island	Groundwater abstraction data in the studied area	Water budget methods tracer tests geochemical methods or hydrological models	Modeling tools or expert judgment	1—Approximate estimation of abstraction (<i>C</i>) 2—Using lumped or semi-distributed models to estimate (<i>E</i>)
Pérez et al. (2019)	Six main aquifers in Colombia	An extensive survey in 12 municipalities	A semi-distributed hydrological approximation	Not considered	1—Ignoring (<i>E</i>) 2—Using semi-distributed models to estimate (<i>R</i>) 3—Calculating (<i>C</i>) through the questionnaires
Esnault et al. (2014)	Two aquifers in the USA	Water balance model (the LPJmL model) and USGS water use survey	Global and local hydrological model (PCRGLOBWB) and hydrological model (CVHM)	PCR-(GLOBWB)	1—Approximate estimation of (<i>E</i>) and calculation based on recharge percentage
This paper	An aquifer located in the central part of Iran	GMS ^a software	GMS software	GMS software	1—Using a numerical distributed model to estimate all three primary parameters of groundwater footprint 2—The possibility of determining high-stress spots in the small scale of an aquifer 3—The possibility of spatial and temporal distributions analysis of high-stress spots and proving proper approaches in the small area to improve the condition

^aGround water modeling system

city in the southeastern part of Tehran. There are several reasons for choosing this study, such as population growth in Tehran, drought periods, reduction in surface water resources, and high dependency of urban and agricultural sectors on groundwater in Varamin plain. Remarkable water demands and uncontrolled groundwater exploitation have led to decline of groundwater level in the

Varamin aquifer in recent years, resulting in land subsidence and groundwater table level decrement (Valivand et al. 2019).

The aquifer is an alluvial unconfined aquifer with an area of 1042.8 km². Figure 1 depicts the study area, which is an arid region with average annual precipitation of 150 mm. Today, the area has become one of the most critical plains of Iran in

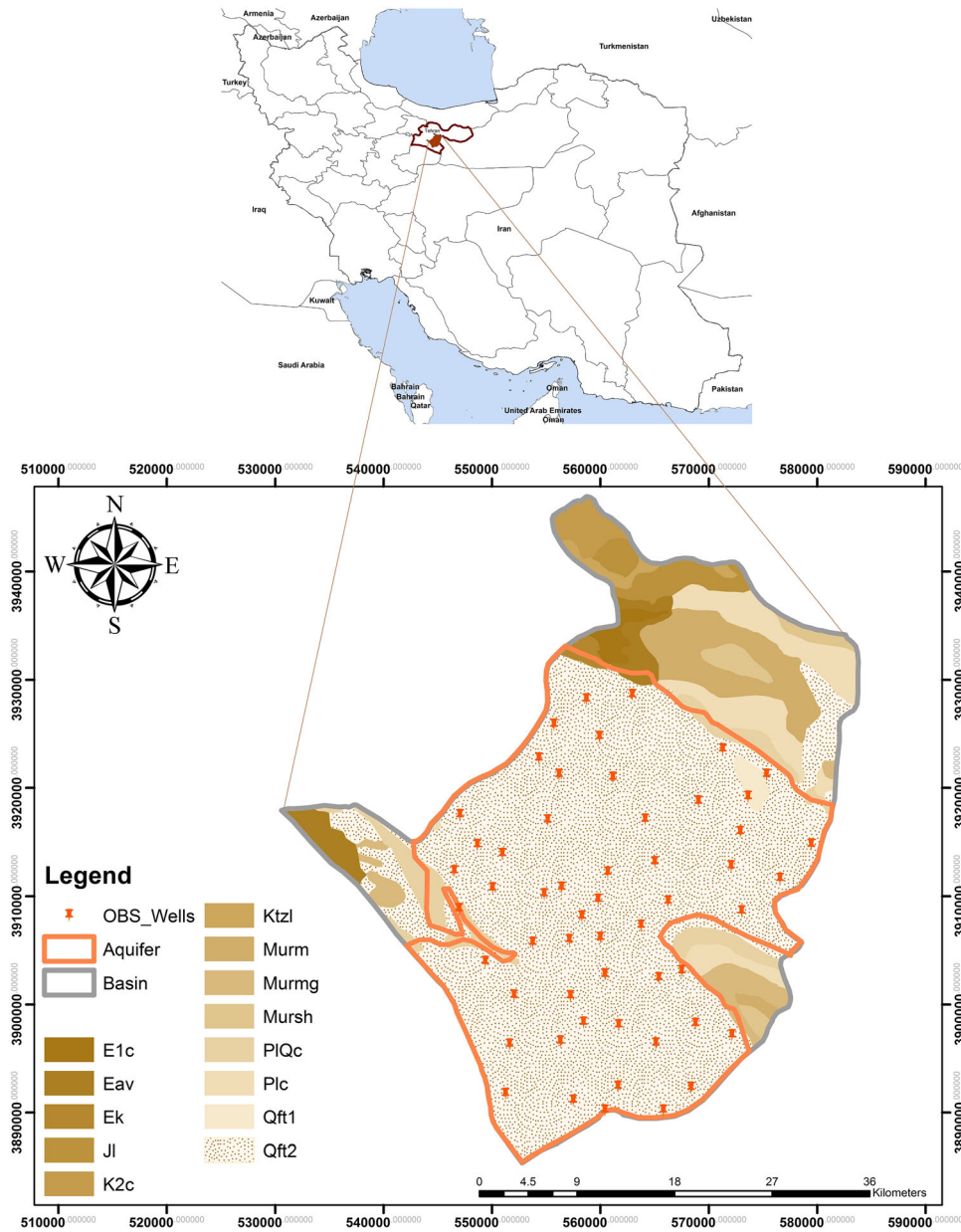


Figure 1. Location and boundary condition of the Varamin aquifer.

terms of the groundwater stress. Figure 2 illustrates the changes in groundwater level in the Varamin aquifer during the period 1989–2015. As shown in this figure, the average groundwater level has decreased 1.35 m annually during the 26-year period, which has caused considerable land subsidence throughout the plain. Therefore, it is necessary to evaluate GWSI precisely to provide strategies useful

for decreasing groundwater loss in the Varamin aquifer.

Geological Setting

The study area consists of a variety of formations, mostly sandstone, shale, and marl, of Eocene to Quaternary ages. A large part of the Varamin

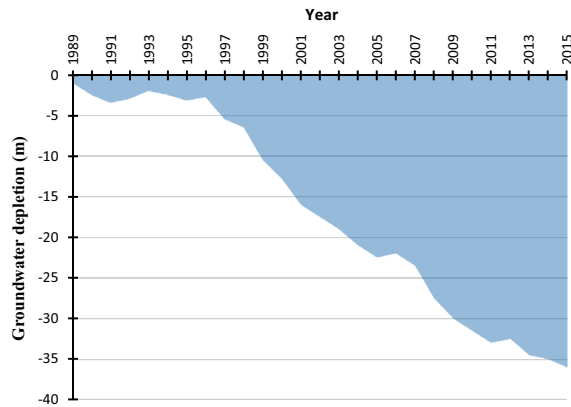


Figure 2. Changes in groundwater level in the Varamin aquifer during the period 1989–2015.

plain lies on an alluvial aquifer, the thickness of which decreases from the northwest to south of the study area (Nejatijahromi et al. 2019).

Hydrogeology

The geophysical data obtained from observation wells reveal that the Varamin plain consists of some important geophysical parts, among which a deep aquifer, a shallow unconfined aquifer, and several perched water units can be recognized. The deep aquifer, as a vast groundwater resource, is extended throughout the plain. The shallow unconfined aquifer is located in the southern half of the plain, while the local perched water units are located in the northern half. The deep aquifer is assumed to be unconfined and confined in the northern and southern halves of the plain, respectively (Mahmoudi et al. 2017). Although the actual boundary of the deep aquifer is not completely determined (Valivand et al. 2019), some previous studies have modeled the aquifer as an unconfined layer (Nejatijahromi et al. 2019; Mohebbi Tafreshi et al. 2019; Nakhaei et al. 2019).

Based on the observations, the transmissivity is not similar in the northern and southern halves of the deep aquifer (Atarzadeh et al. 2014). However, the transmissivity decreases toward the southern half because of the remarkable variations in aquifer thickness, as well as sediment particle size (Mohebbi Tafreshi et al. 2019).

Groundwater Stress

To determine groundwater stress based on groundwater footprint considering the principal parameters of groundwater abstraction, recharge rate, aquifer area, and the groundwater quantity contributing to environmental flow, the following equation is used:

$$WSI = \frac{GWFI}{A_A} = \frac{C}{(R - E)} \quad (1)$$

where GWSI is the groundwater stress index, GWFI is the groundwater footprint index, C is the groundwater abstraction (m^3/day), R is the recharge rate (m^3/day), A_A is the aquifer area (m^2), and E is the environmental flow requirements (m^3/day). Gleeson et al. (2012) state that if GWSI is less than one ($GWFI/A_A < 1$), then groundwater stress is negligible; if GWSI is larger than one ($GWFI/A_A > 1$), it is a sign of unsustainable groundwater abstraction, putting pressure on the aquifer as well as the ecosystem due to the abstraction rate in the area. When GWSI is very high ($GWFI/A_A >> 1$), it describes unsustainable groundwater abstraction. The approach proposed by Gleeson et al. (2012) is a reliable method to determine water footprint, which can be used to study the effects of groundwater abstraction.

Data and Methodology

Because this study aims to provide a distributed model to determine groundwater stress in Varamin plain, data of the aquifer (e.g., input and output boundaries of the aquifer, precipitation, pumping and observation wells, bedrock level, aquifer topography, and hydraulic conductivity) were prepared and input into the Groundwater Modeling System (GMS) software (Sheikhipour et al. 2018; Gorgij et al. 2018). After the primary construction of the conceptual model, the steady model was generated. Furthermore, an unsteady model was developed after calibrating and adding information relevant to the specific yield. To simulate seasonal rivers, the river package was added to the model by inserting the shape file of rivers into the model, followed by defining the sections of the river. Relevant data on groundwater level and hydraulic conductivity were embedded in each river section. Finally, the model was recalibrated. Consider-

ing the data required for building a model for the period 2010–2017, and the availability of data on aquifer water budget in 2013, the year 2013 was selected to evaluate groundwater stress. The availability of water budget data in 2013 allows us to compare the GWSI calculated by water budget studies with the index obtained in distributed modeling. In the unsteady model and according to available water table depths in the observation wells, information of 80% of the months was considered for model calibration, while the remaining data were used for model verification.

Based on the water table depth information in the study area, the highest and lowest water levels in consecutive years were observed in March and September, respectively. Thus, the data of these 2 months in 2013 were considered for calculating groundwater stress. GWSI was also evaluated using water budget studies in 2013, and the results were compared with the findings of the GMS software. The data of March and September were analyzed separately in the GMS software, and three main parameters of the groundwater stress (i.e., groundwater abstraction, recharge rate, and environmental flow interacted with groundwater resources) were extracted. The groundwater stress in 2020 active cells was calculated using Eq. (1). Due to river inflow from the northeastern part of the aquifer and outflow from the south of the aquifer, the river–aquifer exchange parameter (E) was calculated only for the cells located in the mentioned direction. After calculating the stress in 2020 cells in March and September of the given year, stress distribution was graphically obtained for these months using the geographic information system (GIS). Then, spatial and temporal distributions of the stress were locally studied in various parts of the aquifer, and the cause of the stress variation was evaluated. To assess the relationship between stress and land use, the stress distribution map was analyzed and evaluated in the study area. Finally, the relationship between stress and subsidence ratio, throughout the aquifer, was studied considering the land subsidence map of the plain. The flowchart of the method used in this study is shown in Figure 3.

Simulation and Modeling

The GMS software package with modular finite-difference flow (MODFLOW) code was utilized to simulate the study aquifer. The MODFLOW

was developed by the U. Geological Survey (USGS), and it is one of the most popular simulation programs (Paul 2006; Valivand et al. 2019). The MODFLOW code is one of the efficient methods that can reliably solve the groundwater flow equation in water resources management problems. Equation (2) shows the partial differential equation that is solved numerically in this code (Szucs et al. 2009):

$$\frac{\partial}{\partial x} \left(K_{xx} \frac{\partial h}{\partial x} \right) + \frac{\partial}{\partial y} \left(K_{yy} \frac{\partial h}{\partial y} \right) + \frac{\partial}{\partial z} \left(K_{zz} \frac{\partial h}{\partial z} \right) + w = S_s \frac{\partial h}{\partial t} \quad (2)$$

where h is the hydraulic head (L), t is time (T), w is the volumetric flux per unit volume (T^{-1}), S_s is the specific storage of the aquifer (L^{-1}), and K_{xx} , K_{yy} , and K_{zz} are, respectively, the values of hydraulic conductivity (L/T) along the x, y, and z coordinate axes. The term w represents the sources and sinks of groundwater, and its negative and positive values denote extraction and injection, respectively. The information on observation and pumping wells, precipitation, bedrock level, topography, and hydraulic conductivity was used. Figure 4 depicts the groundwater inflows and outflows, along with the locations of the wells. The inflows recharge the Varamin aquifer from the north and generate outflows in the lowest part of the aquifer as well as draining some water out of the aquifer. Out of the 70 observation wells, the data of 54 wells were suitable for aquifer simulation and 3,200 pumping wells were modeled.

Precipitation was considered as an aquifer recharge parameter because the aquifer is recharged by rainfall. The study aquifer is recharged by both precipitation and groundwater inflow, as well as the returning water from drinking, industrial, and agricultural wells. Therefore, considering the type of pumping wells (drinking, industrial, or agricultural), a percentage of abstraction is considered as aquifer recharge. The percentages for drinking, industrial, and agricultural sections are 15, 4, and 81%, respectively (Nadiri et al. 2014). October 2010, as beginning of water year, was selected as the steady period to calibrate hydraulic conductivity, while the unsteady period was considered from November 2010 to December 2015, and a specific yield was reached for the final calibration. The period from January 2016 to April 2017 was considered for

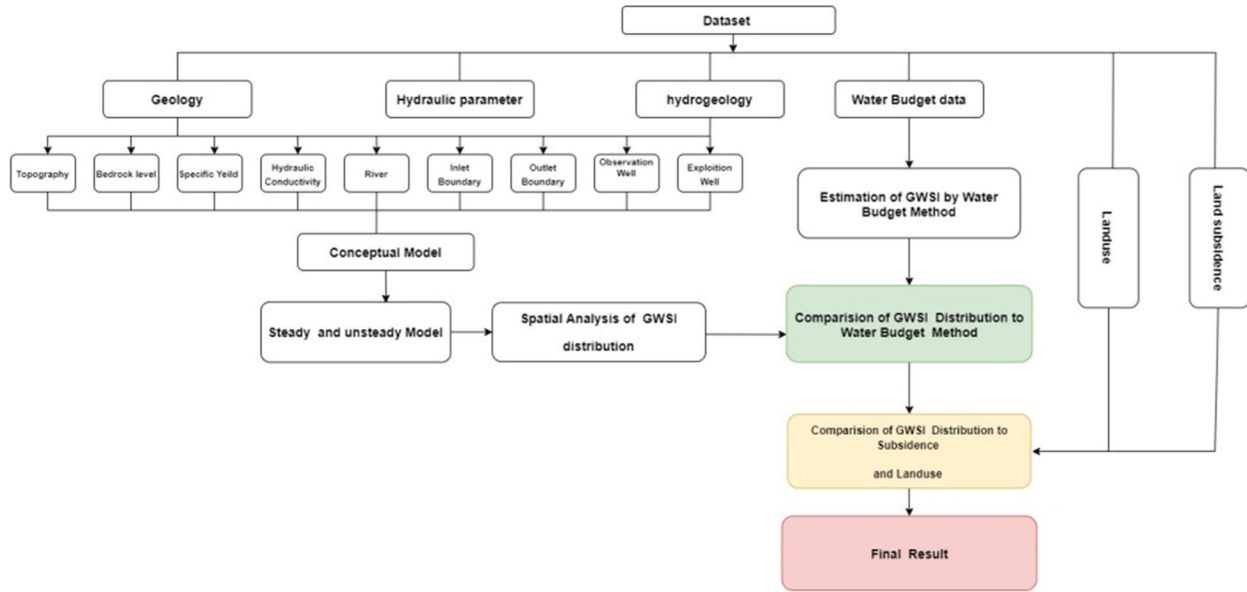


Figure 3. Flowchart of the method used in this study.

model verification. Figure 4 shows the conceptual model, including the observation wells, inputs and output flows, river, and boundary of the aquifer.

For the determination of the discharge in various points of the aquifer, available data of flows from the pumping wells, along with their local information, were used to enter GIS files into the GMS. Besides, the output boundaries of the model were considered based on water budget studies. Water table depth maps obtained by water budget studies were used to determine the recharge values of the aquifer inflows. Then, recharge flow by rainfall and return flow were calculated in different parts of the aquifer. For model calibration in observation wells, the aquifer was divided into 21 subareas with various recharge rates, which was further used for spatial analysis. Table 2 shows the error in steady and unsteady models.

The groundwater contributed to the environmental flow was obtained by calculating streamflow from the aquifer to the river. Therefore, a seasonal river was considered in the final unsteady model and calibration process. River–aquifer exchange measured in cells of the distributed model, which crossed the river and aquifer outflow to the river, was inserted to water balance. In global hydrological or non-distributed models, E is obtained as a fraction of R , according to Eq. (3), where Q_{90} is the monthly

streamflow that exceeds 90% of the time and Q_{ave} is the long-term average streamflow.

$$E = \frac{Q_{90}}{Q_{ave}} \quad (3)$$

E is the exchange ratio of the aquifer and river, which includes aquifer inflows or outflows. The distributed models can be used to predict the exact value of E .

A distributed model was used in this study where groundwater budget balance was considered separately for each cell. The groundwater leakage rate in the unsteady model was calculated in each cell crossed by the river, and the effects of E were precisely considered in stress calculations. Finally, by obtaining three main parameters of the model, stress was determined using Eq. (1) for all cells. Based on Gleeson’s classification, the stress was divided into five categories. The cells with stress index lower than one are considered as ‘without stress,’ whereas the values between 1 and 5 demonstrate ‘moderate stress.’ Furthermore, values between 5 and 10 indicate ‘high stress’ and between 10 and 20 ‘severe stress.’ Finally, the cells with values more than 20 are ‘under critical water stress’ (Gleeson et al. 2012).

Table 2. Errors calculated in steady and unsteady model

Model	Mean error (m)	Mean absolute error (m)	Root-mean-square error (m)
Steady	– 0.18	0.71	0.84
Unsteady	– 0.1	0.9	1.08

RESULTS AND DISCUSSION

Simulation Results

Figure 5 shows the locations of observation wells and groundwater contours after calibration in the unsteady state. The observed and simulated values of groundwater level in the observation wells in the aquifer were compared, for four arbitrary wells, coded by the numbers of 6, 9, 57, and 72 (Fig. 6). According to Figure 6, which belongs to the model verification period, the average differences between the observed and simulated levels in the verification period were 1.10, 0.55, 0.49, and 1.12 m in wells 6, 9, 57, and 72, respectively, which are negligible. These small errors in groundwater level calculations show the efficiency of the groundwater simulation model.

Groundwater Budget Model for GWSI Estimation

In hydrology, the term water balance is used to describe the continuous water inflow and outflow in a system. Groundwater budget is defined based on the water balance that considers the inflow and outflow, as well as the changes in groundwater storage. Measuring these variables in a groundwater system is more complicated than that in a surface water system. Due to the effects of lots of influential factors on groundwater balance, even if a complete dataset is available, it is not possible, or at least it is difficult, to measure some of these effective factors in the groundwater balance equation. Therefore, only by relying on the hydrological conditions of the aquifer, the parameters in the water budget equation can be estimated approximately. Equation (4) shows how groundwater balance in an aquifer is calculated:

$$\text{Aquifer storage changes} = \text{Aquifer inflow} - \text{Aquifer outflow}. \quad (4)$$

The influential factors on inputs of the system in the groundwater balance equation include under-

ground inflow coming from the mountainous and upper elevations, as well as recharge from the aquifer surface. On the other hand, the influential factors on outputs of the system include groundwater abstraction wells, Qanats, alluvial springs of the aquifer, evaporation from the aquifer (in areas where water table depth is close to the earth surface), natural or artificial aquifer drainages, and underground outflow from the aquifer. Three main groundwater parameters in Eq. (1) were determined and measured based on the water budget model for the Varamin aquifer in this study. Then, groundwater stress was calculated in the desired year, as indicated in Table 3.

For water budget, studies reveal that by applying the values in Table 3 in Eq. (1) the groundwater stress index for the Varamin plain is 1.31. As can be seen, the measured value represents the groundwater stress in the desired aquifer. However, comparing the results with the results of spatial distributed modeling in the next section reveals that water budget studies show much less stress value. Furthermore, the distribution of stress, as well as the determination of non-critical and unstressed areas, cannot be determined exactly using the budget-based approach. Most of the parameters in simple groundwater balances have been determined by expert comments and engineering judgments that consider uncertainty. Therefore, the results of the distributed model in the groundwater stress determination are more reliable than water budget estimation. Several studies have compared the distributed models with simple groundwater balances. Bredehoeft (2002) stated that the principal method for showing a dynamic process in an aquifer system is groundwater modeling; he showed that sustainable use of groundwater resources cannot be achieved by applying only simple groundwater balances. His findings revealed that available groundwater and the aquifer responses to abstraction and recharge can only be approximated with precise groundwater modeling. The groundwater models can simulate the impact of withdrawals on ground-

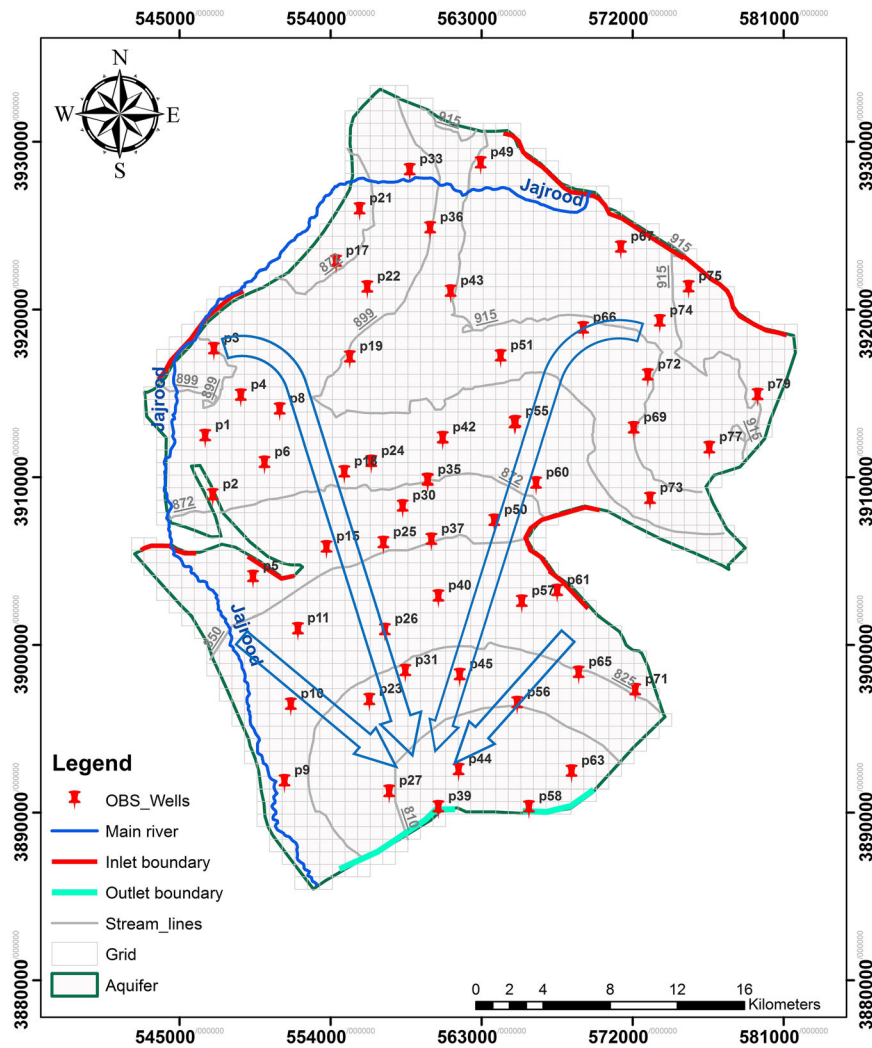


Figure 4. Conceptual model of this study.

water flow, streamflow, and water budgets by considering the withdrawal locations and magnitudes as the model inputs. These models can estimate GWSI more efficiently than the groundwater budget method. In addition, groundwater modeling considers the flow directions, changes in water levels and aquifer storage, and other hydrologic processes, caused by withdrawals (Goode 2016). These benefits are ignored in simple groundwater balances.

Spatial Distribution of GWSI

As mentioned earlier, previous studies have tried to determine GWSI on a regional scale by applying either the global hydrological models or

water budget methods. For example, Gleeson et al. (2012) determined the global groundwater footprint mapping of regional aquifers all over the world. Although there are limited studies on numerical modeling and stress calculation based on the distributive assessment of groundwater footprint, the present study attempts to determine the stress index and footprint to compare the results of modeling with water budget results. The results showed that stress calculation using global hydrological models or water budget methods on a large scale offers different results in comparison with numerical modeling. Similar to the results of this study, Goode (2016) denoted that global models might be less useful at watershed or sub-basin scales. Therefore, in both large and small scales of the aquifer, the dis-

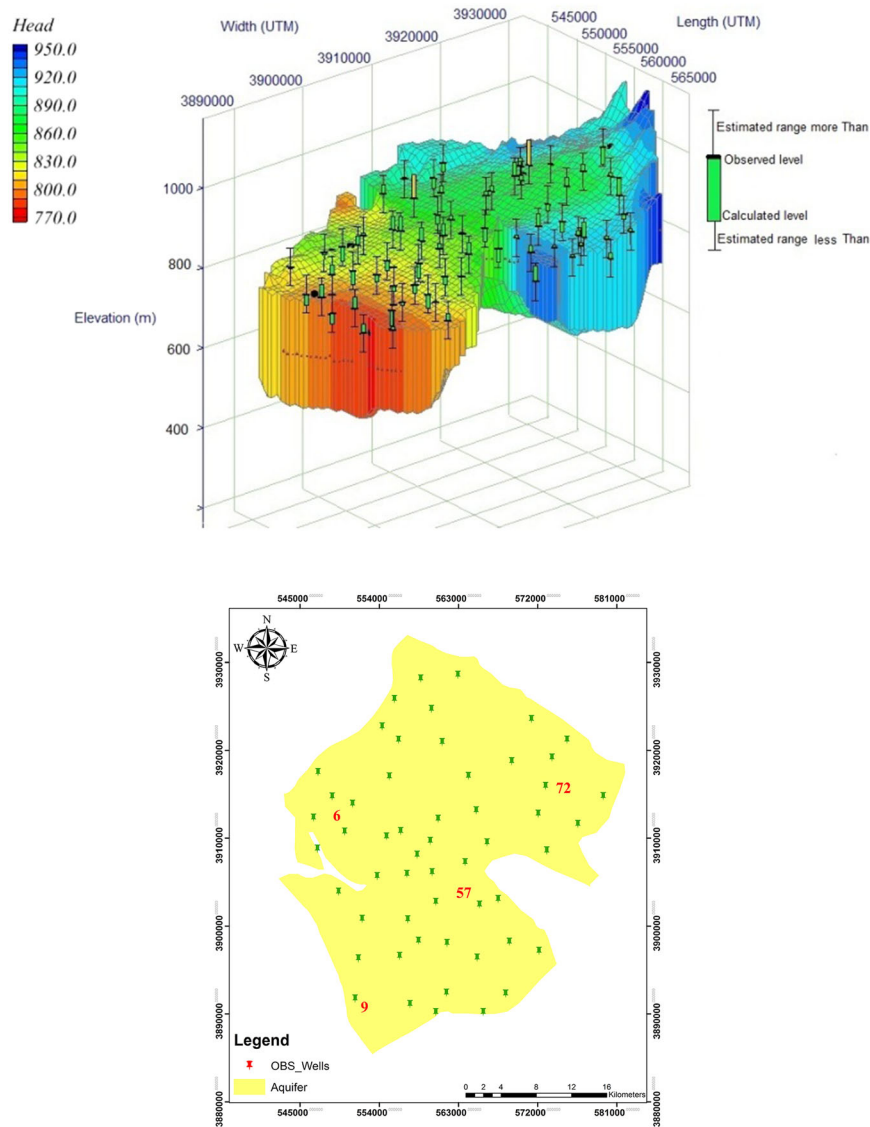


Figure 5. Calibrated observation wells and simulated groundwater level in the unsteady state.

tributed models are more precise than global models and water budget methods.

Due to heterogeneity in eco-hydrological systems, water consumption in local and regional basins can have significant effects on the results. The groundwater stress obtained by the distributed modeling in the studied aquifer confirms the issue discussed in the following section. Therefore, by determining the distributed GWSI, the footprint map is prepared. Footprint map is an efficient analytical tool where groundwater flow modeling or other hydrologic methods can be utilized to deter-

mine the effects of large amounts of groundwater and surface water withdrawal (Goode 2016).

For this purpose, at first, the months with the highest and lowest groundwater levels were determined during 2013 based on water table depths recorded in the observation wells. Then, the distributed model was used for these months, and water stress was obtained. Accordingly, abstraction, recharge, and water exchange between the river and aquifer were determined, and stress values were calculated for March and September using Eq. (1) in the studied year for all the cells throughout the aquifer.

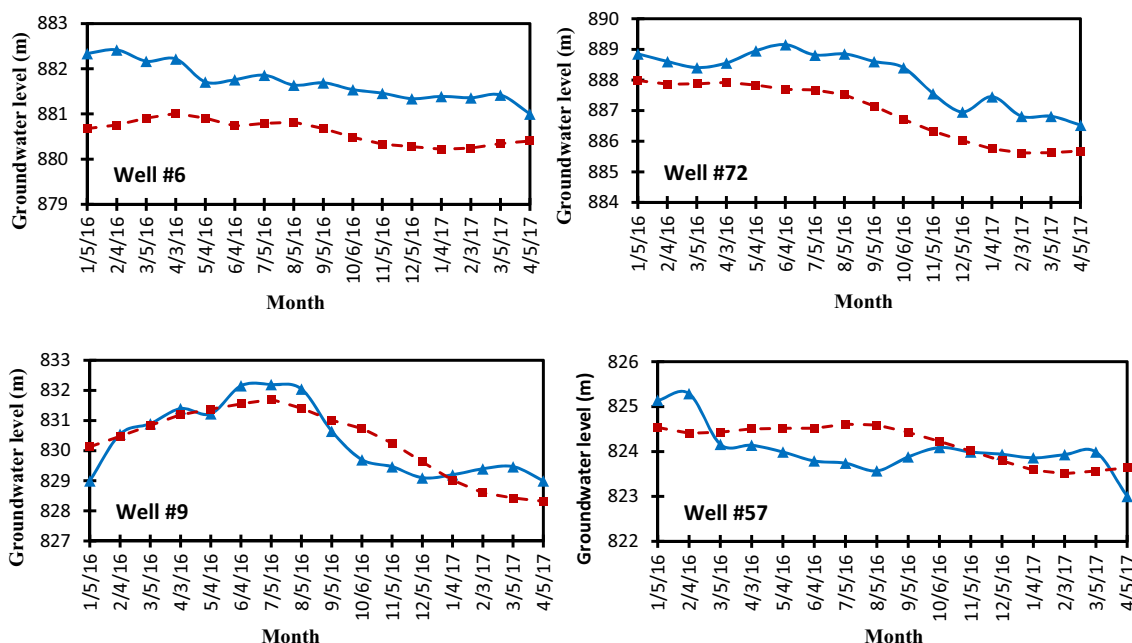


Figure 6. Observed and simulated groundwater levels for four arbitrary wells coded with numbers of 6, 9, 57, and 72, respectively.

Table 3. Estimation of groundwater stress index based on water budget data

Total aquifer inflow factors, mm ³ /year	$\sum R = 380$
Total aquifer outflow factors, mm ³ /year	$\sum C = 472$
Total environmental requirement, mm ³ /year	$\sum E = 20$
Groundwater footprint index, km ²	1366.0
Groundwater stress index	1.31

In Figure 7, the results of GWSI are compared for March and September 2013 in the Varamin aquifer. Ten zones out of all 21 zones are illustrated with more details. According to precipitation data recorded by rain gauge stations in the study area, the difference in precipitation amount for March and September in the desired year was 389 mm. As shown in Figure 7, in almost all 21 zones of the aquifer, five classes of Gleeson et al. (2012) with various density rates are observed. Table 4 shows the groundwater stress evaluation in March and September with more details in 2013. For comparison, the stress range is divided into five categories, according to Gleeson et al. (2012). The percentage of cells with different stress ratings is given for 2 months of 2013, with the highest and lowest water table depths.

According to Table 4, the calculated stress throughout the basin in March for the desired year is

less than that in September. Moreover, because of the precise distributed modeling, the mean water stress in the distributed model varies with the value obtained by applying the water budget model presented by Gleeson et al. (2012) for the aquifers of Iran. Gleeson et al. (2012) estimated GWSI for the studied aquifer from 11.1 to 28.3. However, the values calculated by the distributed model were higher than these amounts and showed one and a half times change between March and September. For instance, the averaged water stress in March and September was obtained 26.51 and 39.39 for the desired year, respectively. Moreover, Table 4 indicates that during the studied months, most parts of the aquifer area faced no water stress, i.e., their GWSI values were less than 1, while for a partial part, severe stress was detected. Comparing the coverage percentage of the five classifications for water stress during the months with high and low water table depths (Table 4) reveals that there are no significant differences in the aquifer coverage percentage for the areas with water stress higher than 1 during 2013. Table 4 illustrates that ~ 45% of aquifer area was under the water stress in March during the studied year and this ratio reached 54% during September, the critical month, which shows stressed areas increased by nearly 9% during

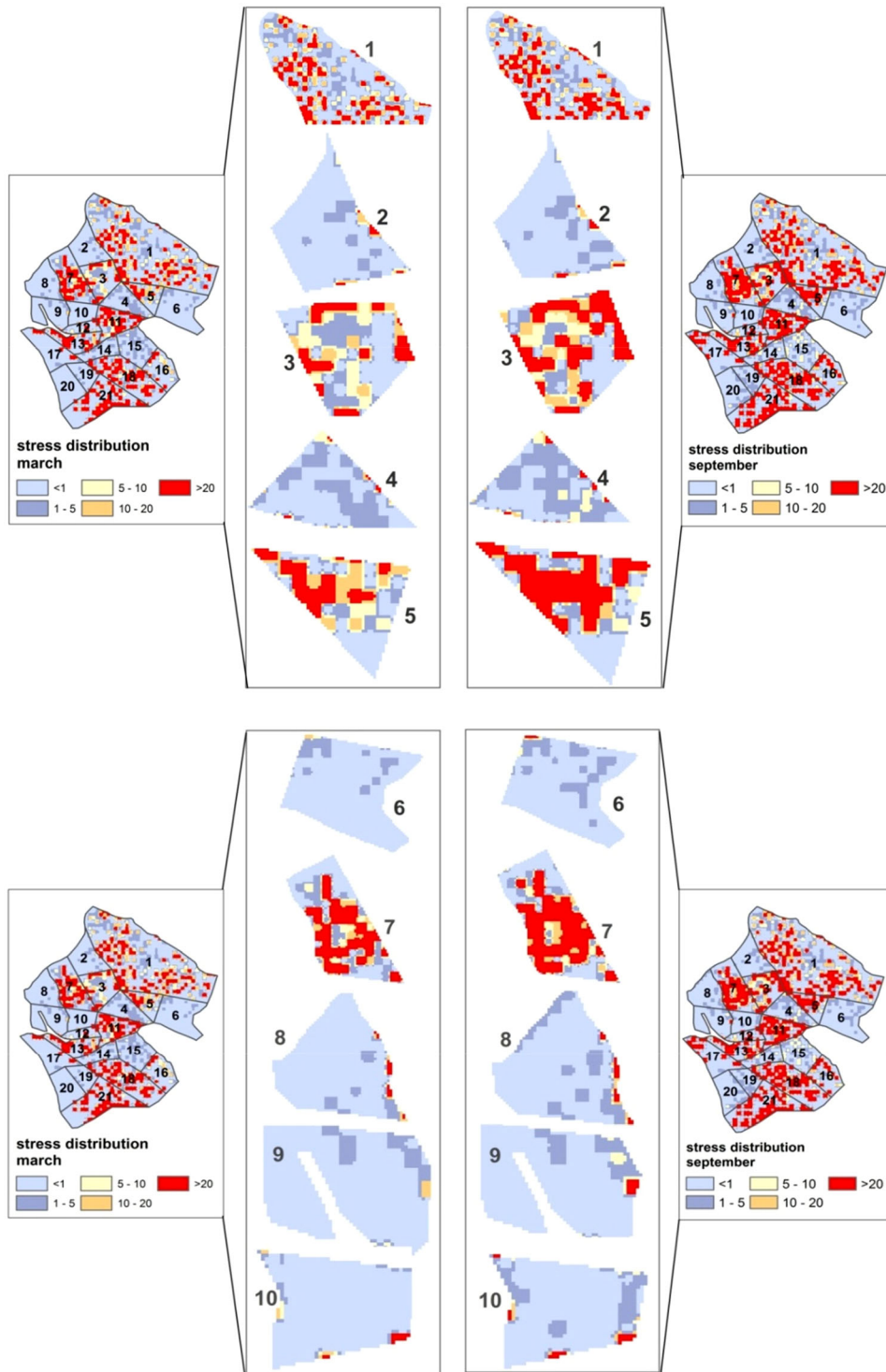


Figure 7. Comparison of groundwater stress distribution in March and September 2013.

Table 4. Percentage of stressed area in March and September 2013 according to the Gleeson’s classification

Range of GWSI	Stressed area/total aquifer area	
	March (%)	September (%)
GWSI < 1	55	46
1 < GWSI < 5	16	18
5 < GWSI < 10	6	6
10 < GWSI < 20	6	6
GWSI > 20	17	24

the driest month of the year. The findings revealed that the aquifer’s behavior is approximately stable. The GWSI distribution does not change significantly, as shown for the selected 10 zones in Figure 7. Therefore, the temporal distribution of GWSI during the year is not significant.

Figure 8 illustrates the spatial distribution of stress in March 2013. The locations of observation wells, as well as stress distribution mapping, are depicted. Therefore, the relation between GWSI and discharge can be interpreted using this figure. The presence of active operating wells during the

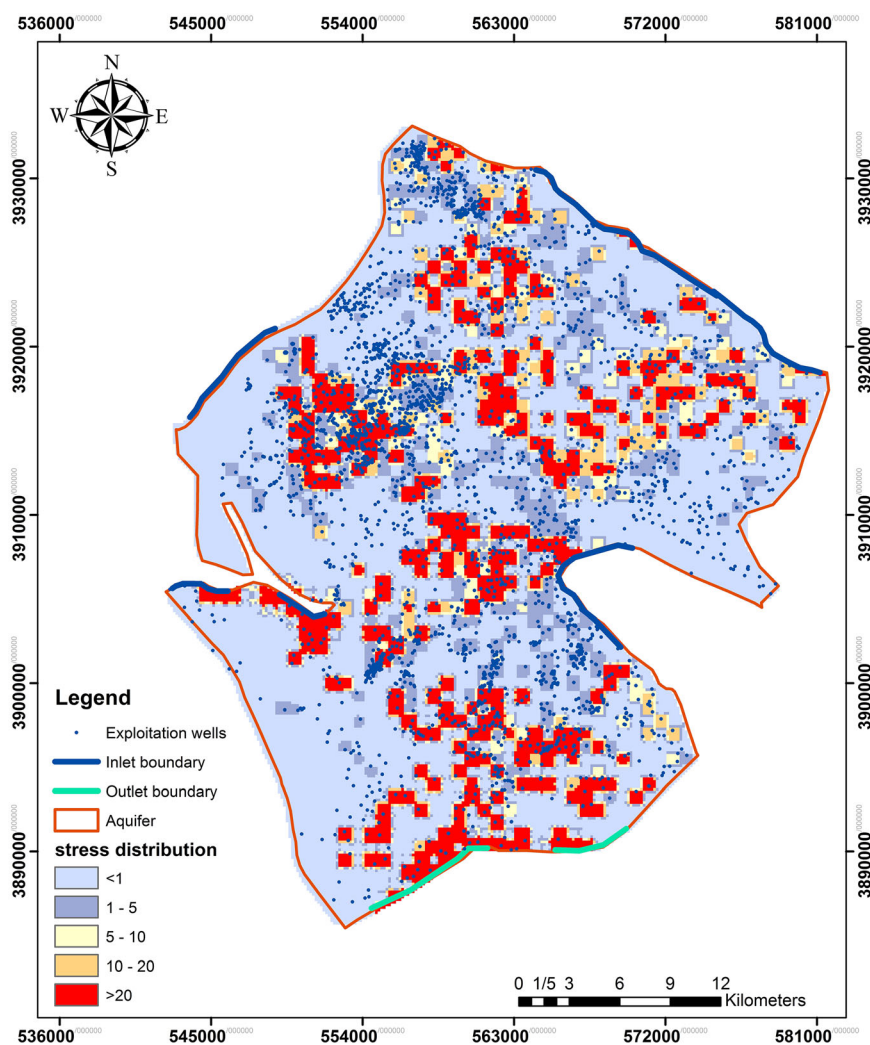


Figure 8. Groundwater stress distribution map with the location of pumping wells in March (2013).

Table 5. Comparison of inflow and outflow values for common highly stressed areas in March 2013

Zone	Abstraction of the operating wells m ³ /day	Boundary inflows and outflows m ³ /day	River m ³ /day	Surface recharge inflow m ³ /day	Area (km ²)	Relative area with GWSI > 20
7	– 32,005	3652	0	981	62	32%
11	– 34,663	1825	0	954	45	40%
18	– 43,327	– 12,501	0	1756	77	33%
21	– 31,619	– 100,568	0	1105	86	27%

year, even in March, and severe abstraction, higher than the recharge rates, results in lots of highly water-stressed cells. In this part of the study, the critical zones with highly stressed spots are analyzed.

According to Figures 7 and 8, in the zones 3, 12, and 16, with no inflow or outflow, low to very critical stresses were observed in the location of wells, depending on the abstraction volume. Besides, the considerable effects of abstraction parameter can be observed in the zones 5, 7, 11, and 13, which demonstrate highly critical stress in many parts despite the vicinity of some parts of their boundaries with groundwater inflows, due to a large number of operating wells, as well as intensive abstractions. Being adjacent to the outflow boundary and having operating wells with intensive abstractions, zones 18 and 21 have a broad highly stressed area.

According to Figure 8 and using the results of GMS software, water balance studies were considered for zones 7, 11, 18, and 21 with high-stress distribution. Regarding the inflow or outflow boundaries crossing some of the allocated cells, the sum of inflows to these boundaries of the cells was calculated in each zone (Table 5). Besides, the total abstraction of the operating wells from these cells categorized as the abstraction of the operating wells was calculated (Table 5). The table also shows the total surface recharge for all cells of the model in each zone as surface recharge inflow. Moreover, the areas with GWSI higher than 20 in each zone, known as highly crucial conditions, are brought in Table 5. Then, the water budget in March 2013 for each of the highly water-stressed zones was evaluated and listed. Table 5 demonstrates that in all four zones, severe abstraction volume resulted in numerous extremely water-stressed cells. Furthermore, because of the considerable amount of groundwater outflow in zone 21, except for the presence of a large number of wells and intense volume of abstraction, extremely water-stressed cells were observed during groundwater simulation.

Due to its vicinity to the outflow boundary, zone 21 has a discharge of 100,568 m³/day, which demonstrates noticeable water stress. In addition, in zone 18, the abstraction volume was 43,327 m³/day, which was very high, and many highly stressed spots were observed. Therefore, excessive groundwater abstraction in the zone creates extremely water-stressed spots with GWSI higher than 20. Therefore, these critical zones with low potential of groundwater should be avoided for agricultural applications, but can be used for industrial infrastructure (Das et al. 2017). As depicted, the stress distribution maps assist authorities with their decisions in allocating the existing and new wells to minimize water stress throughout the basin and prevent the intensification of stress in the aquifer.

Comparison of GWSI and Land use

Land-use pattern in an area is one of the critical factors that control the availability of groundwater (Das et al. 2017). It is one of the influential factors that increase water stress (Banerji et al. 2020). To assess the land use–water stress relation, as well as to study the increasing amount of stress in some regions of the aquifer, land-use maps are presented in Figure 9. According to the water budget data in the studied plain, 89.94, 8.12, and 1.94% of the total volume of surface and underground water in the area are consumed in agricultural, urban, and industrial sectors, respectively. By overlaying the highly water-stressed regions (zones 7, 11, 18, and 21), which were identified in the stress distribution map in Figures 7 and 8, and the land-use map in Figure 9, it is revealed that agricultural and urban lands have the highest groundwater consumption rate with regard to water budget studies, which increases overall water stress throughout the aquifer. Having a more precise overview of the other parts of the plain, overlaying the highly stressed spots in

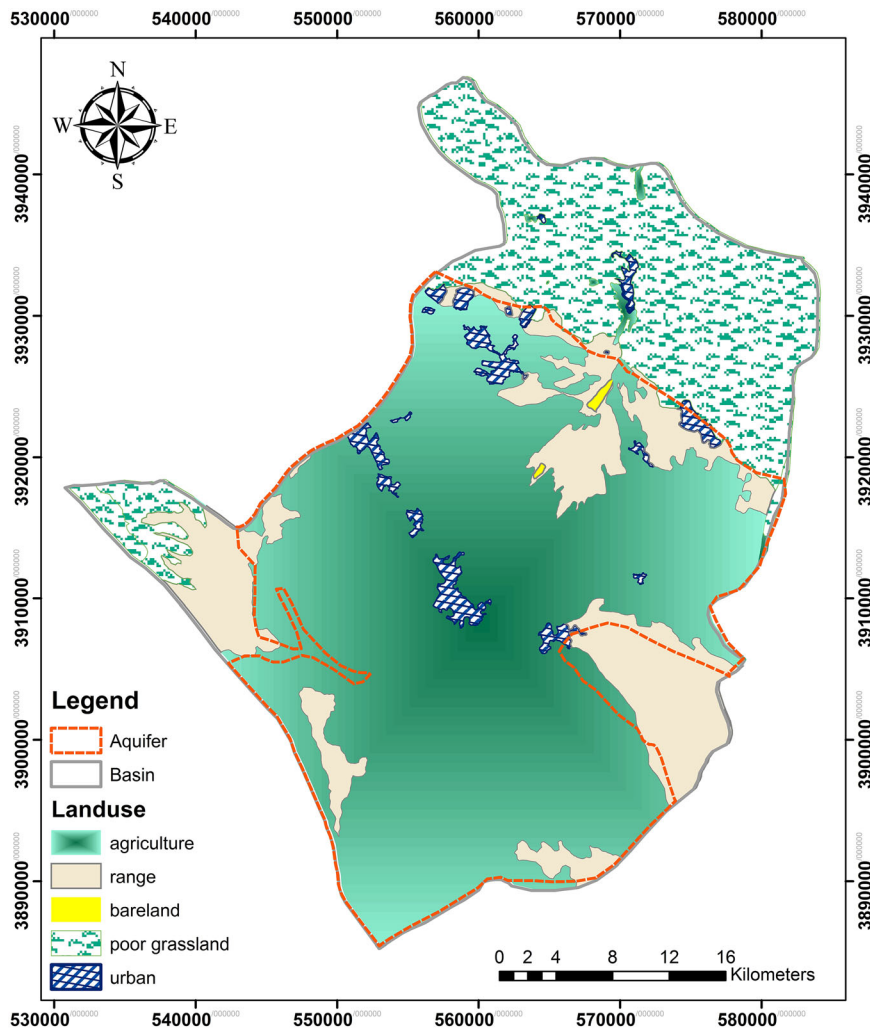


Figure 9. Land use in the Varamin plain.

zones 3, 5, and 13, as well as the southern parts of zone 1 in Figures 7 and 8 and the land-use maps in Figure 9, shows the agricultural farms with high groundwater consumption. According to the GMS software, the amount of groundwater abstraction in highly stressed spots in zones 3, 5, 7, 11, 13, 18, and 21, as well as the southern parts of the zone 1, about 60% of total abstraction over the Varamin plain occurred in March 2013. Therefore, the potential of spatial stress distribution maps to detect highly stressed regions, as well as their significant role in proposing strategies to reduce stress by modifying land-use patterns, was determined. In contrast, the water budget model's calculations cannot detect highly stressed points in a distribution map or assess an efficient spatial analysis. The distributed model

aids authorities to reduce aquifer water stress in critical regions of the basin using tools, such as collaborations with farmers, to change cultivation patterns or decreasing the abstraction of the wells in the highly stressed region. These methods, in the form of specific long-term scenarios for agricultural lands, make it possible to have a non-stressed basin without controversial water crises.

Comparison of GWSI and Subsidence

Mohebbi Tafreshi et al. (2019) proposed that lithologies and formations, which contain fine-grained materials such as clay and silt in their structure, increase the rate of subsidence. Clayey or

sandy soils create unstable conditions that increase the probability of instantaneous land subsidence phenomenon. A notable volume of soil material in the study includes soil particles that increase the probability of land subsidence occurrence in the aquifer. Moreover, other parameters, such as being located in arid and semiarid regions, increase the possibility of land subsidence in the study area (Momeni et al. 2012). On the other hand, the more the abstraction volume from the aquifer, the more the effective stress on soil layers, which could lead to an increase in the probability of land subsidence phenomenon throughout the plain (Jafari et al. 2016). Guzy et al. (2020) reported that land subsidence is likely one of the most obvious environmental effects of groundwater pumping. They showed that this phenomenon increased up to 14.5 m by increasing the aquifer abstraction.

In the following, the correlation of highly stressed zones and land subsidence is discussed by comparing the stress map in March 2013 in Figures 7 and 8 and the land subsidence map in Figure 10. Investigations on soil material of the studied plain show a vast number of clayey and silty layers throughout a large of the plain area from its north to south. In the long term, the water table depth declines due to the severe abstraction of the aquifers composed of silty and semi-compacted clayey layers with an appropriate thickness. Severe water abstraction causes sudden water release of densely impenetrable aquifers in the form of land subsidence. Furthermore, this phenomenon can be observed in some parts of the studied aquifer with fine soil materials consisting of silt and clay (Galloway et al. 1998).

Observations and field assessments indicated that the two influential factors responsible for the occurrence of land subsidence are intensive groundwater abstraction and material thickness of the sedimentary layers in the study area. According to geotechnical and geological field studies, various parts of the zone 1 are composed of two distinct soil types (Fig. 8). The northern parts consist of large-sized sandy sediments with extremely high hydraulic conductivity. Furthermore, the central and southern parts of the zone 1 consist of large and medium sandy sediment layers with thick layers of clay in between. Therefore, according to Figure 10, due to the low thickness of fine soil layers in zone 1, the high values of land subsidence were not observed. Although zone 11 is confronted with intensive groundwater abstraction and has many highly

stressed points, sandy soil in this zone caused only small land subsidence in its southern parts. However, zones 7, 8, 9, 10, 12, 13, 17, and 20 consisted of fine sand materials with low-thickness clayey layers. The high groundwater level in western and southwestern regions of the aquifer, as well as low thickness of alluvial fine sediments, resulted in the insusceptibility of the above-mentioned areas to maximum land subsidence.

As a result, high groundwater stress due to intensive abstraction in some regions, such as zones 7 and 13, did not lead to maximum land subsidence. Zones 2 and 3 consisted of a combination of fine sandy and clayey materials. Besides, zones 4 and 5 include medium-sized and fine sediments, where the thickness of clayey layers increases as proceed toward the southern parts. Finally, zone 6 consists of fine silty and clayey materials.

In some parts of zones 2, 4, and 6, due to the presence of soil having silty and clayey sediments with high vulnerability to land subsidence, despite relatively low amounts of groundwater stress, the maximum land subsidence was observed. In zones 3 and 5, the presence of fine-sized materials susceptible to land subsidence and intensive groundwater abstraction also increased the land subsidence. Moreover, according to geological surveys, zones 14, 15, 16, 18, 19, and 21 have a wide range of fine-sized sediments mixed with clayey materials, demonstrating finer materials as proceed toward the southern part of the plain that only silt and clay are observed. Condition and type of the soil in the southern parts of the Varamin plain increased the land subsidence because of a massive decline in water table depth. Therefore, it can be stated that high amounts of stress, solely, cannot be responsible for increasing the risk of land subsidence in the region. The thickness of the clay layer and over-pumping in southern and central parts of this plain cause more risk of subsidence in these zones (Mohabbi Tafreshi et al. 2019). The correlation between the area under subsidence and the groundwater stress is depicted in Figure 11. According to the figure, 31.55 and 27.45% of the aquifer area is only under groundwater stress and land subsidence, respectively. Figure 11 indicates that 25% of the aquifer area is under both stress and subsidence. Furthermore, 63% of this area includes highly stressed spots with GWSI values more than 20, and the subsidence rates more than 6 cm. This area covering ~ 16% of the aquifer area is exposed to a

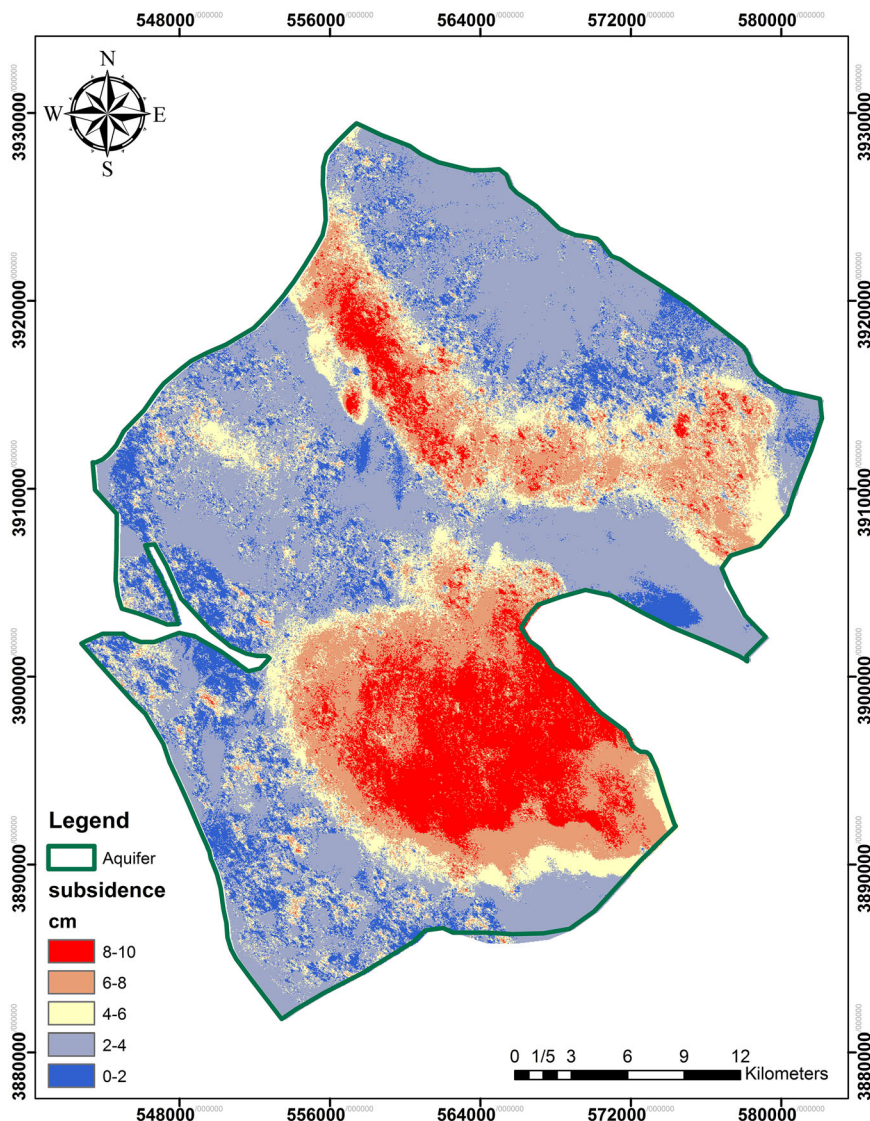


Figure 10. Land subsidence rate (cm) in Varamin plain.

high risk of subsidence, and management scenarios are required to protect the area.

CONCLUSION

Since intensive groundwater abstraction leads to water table depth decline and several consequences, such as land subsidence, it is crucial to define some criteria to evaluate the stress of groundwater resources. In this study, the groundwater stress criterion was defined based on the novel concept of groundwater footprint. Using the GMS

distribution approach, three fundamental parameters in the groundwater stress equation were estimated for the areas smaller than 1 km² in the aquifer. The distributed model exerted a better performance in the evaluation of groundwater stress compared to the water budget approach. Moreover, the calculations based on the water budget approach resulted in a different conclusion about stress in the studied aquifer compared to the distributed model. The minimum and maximum averaged values calculated for the GWSI by the distributed model were 2.4 and 1.4 times, respectively, more than the GWSI values obtained by previous studies on this aquifer.

PERCENTAGE OF AREA UNDER STRESS AND SUBSIDENCE

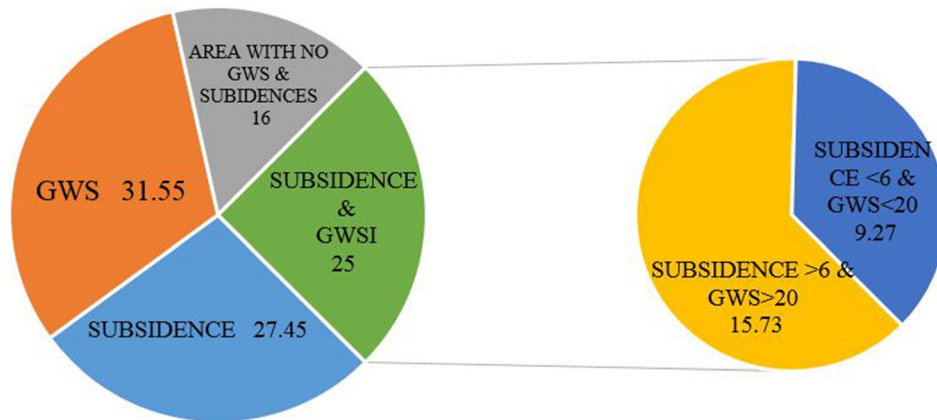


Figure 11. Aquifer areas under groundwater stress and land subsidence.

The findings demonstrate that during analysis of groundwater stress, distributed modeling provided more accurate results compared to the water budget approach because the parameters in distributed modeling are determined and calibrated based on observation data, which can minimize uncertainty of the parameters by considering their physical nature. Moreover, by using land-use maps, the high stressed regions were assessed, and the correlations between these regions with areas affected by land subsidence were studied.

The results showed that highly water-stressed regions exert a direct meaningful correlation with agricultural land use and intensive groundwater abstraction. Stress in the aquifer can be managed and reduced through mitigation plans, such as changing cultivation patterns and relocating agricultural farms in the basin. Comparative studies on water stress and land subsidence throughout the aquifer show that, in general, an increase in groundwater stress does not always increase the land subsidence risk in the basin, and soil materials are more influential on land subsidence. Results showed that 40% of the aquifer is exposed to land subsidence. In the area under subsidence, between the two factors of soil material and groundwater stress, soil material played the main role, whereas groundwater stress participated in the subsidence by only 10%. The stress distribution concept pursued in this study is helpful for groundwater resource managers on the local abstraction deduction of aquifers, especially in areas where land subsidence is sub-

jected to overexploitation due to soil material (zones 3 and 5) to prevent increasing the land subsidence. Furthermore, in the southern parts of the aquifer, that soil material is susceptible to land subsidence, and water table depth is remarkably low (zones 14, 15, 16, 18, and 21), applying artificial recharge is a suitable solution in preventing land subsidence in the regions. Therefore, applying appropriate scenarios in the future can prevent water stress or, at least, reduce its intensity.

REFERENCES

- Al-Naeem, A. A. (2014). Effect of excess pumping on groundwater salinity and water level in Hail region of Saudi Arabia. *Research Journal of Environmental Toxicology*, 8(3), 124.
- Atarzadeh, A. A., Tavana, B., & Abrazi, B. (2014). *Quantitative and contamination studies of Varamin aquifer (groundwater studies)*. Tehran: Yekom Consulting Engineering.
- Banerji, S., Biswas, M., & Mitra, D. (2020). Semi-quantitative analysis of land use homogeneity and spatial distribution of individual ecological footprint in selected areas of Eastern fringes of Kolkata, West Bengal. *Geocarto International*, 35(1), 78–92.
- Bredehoeft, J. D. (2002). The water budget myth revisited: Why hydrogeologists model. *Groundwater*, 40(4), 340–345.
- Das, S. (2019). Comparison among influencing factor, frequency ratio, and analytical hierarchy process techniques for groundwater potential zonation in Vaitarna basin, Maharashtra, India. *Groundwater for Sustainable Development*, 8, 617–629.
- Das, S., Gupta, A., & Ghosh, S. (2017). Exploring groundwater potential zones using MIF technique in semi-arid region: A

- case study of Hingoli district, Maharashtra. *Spatial Information Research*, 25(6), 749–756.
- Das, S., & Pardeshi, S. D. (2018). Integration of different influencing factors in GIS to delineate groundwater potential areas using IF and FR techniques: A study of Pravara basin, Maharashtra, India. *Applied Water Science*, 8(7), 197.
- Das, S., Pardeshi, S. D., Kulkarni, P. P., & Doke, A. (2018). Extraction of lineaments from different azimuth angles using geospatial techniques: A case study of Pravara basin, Maharashtra, India. *Arabian Journal of Geosciences*, 11(8), 160.
- Dumont, A., Salmoral, G., & Llamas, M. R. (2013). The water footprint of a river basin with a special focus on groundwater: The case of Guadalquivir basin (Spain). *Water Resources and Industry*, 1, 60–76.
- Esnault, L., Gleeson, T., Wada, Y., Heinke, J., Gerten, D., Flannery, E., et al. (2014). Linking groundwater use and stress to specific crops using the groundwater footprint in the Central Valley and High Plains aquifer systems, US. *Water Resources Research*, 50(6), 4953–4973.
- Galloway, D. L., Hudnut, K. W., Ingebritsen, S. E., Phillips, S. P., Peltzer, G., Rogez, F., et al. (1998). Detection of aquifer system compaction and land subsidence using interferometric synthetic aperture radar, Antelope Valley, Mojave Desert, California. *Water Resources Research*, 34(10), 2573–2585.
- Gambolati, G., & Teatini, P. (2015). Geomechanics of subsurface water withdrawal and injection. *Water Resources Research*, 51(6), 3922–3955.
- Goode, D. J. (2016). Map visualization of groundwater withdrawals at the sub-basin scale. *Hydrogeology Journal*, 24(4), 1057–1065.
- Gleeson, T., & Wada, Y. (2013). Assessing regional groundwater stress for nations using multiple data sources with the groundwater footprint. *Environmental Research Letters*, 8(4), 044010.
- Gleeson, T., Wada, Y., Bierkens, M. F., & Van Beek, L. P. (2012). Water balance of global aquifers revealed by groundwater footprint. *Nature*, 488(7410), 197–200.
- Gorgij, A. D., Kisi, O., Moayeri, M. M., & Moghaddam, A. A. (2018). Hydraulic conductivity estimation via the AI-based numerical model optimization using the harmony search algorithm. *Hydrology Research*, 49(5), 1669–1683.
- Guzy, A., & Malinowska, A. A. (2020). State of the art and recent advancements in the modelling of land subsidence induced by groundwater withdrawal. *Water*, 12(7), 2051.
- Jafari, F., Javadi, S., Golmohammadi, G., Karimi, N., & Mohammadi, K. (2016). Numerical simulation of groundwater flow and aquifer-system compaction using simulation and InSAR technique: Saveh basin, Iran. *Environmental Earth Sciences*, 75(9), 833.
- Kourgialas, N. N., Karatzas, G. P., Dokou, Z., & Kokorogiannis, A. (2018). Groundwater footprint methodology as policy tool for balancing water needs (agriculture and tourism) in water scarce islands-The case of Crete, Greece. *Science of the Total Environment*, 615, 381–389.
- Mahmoudi, N., Nakhaei, M., & Porhemmat, J. (2017). Assessment of hydrogeochemistry and contamination of Varamin deep aquifer, Tehran Province, Iran. *Environmental Earth Sciences*, 76(10), 370.
- Minderhoud, P. S. J., Coumou, L., Erban, L. E., Middelkoop, H., Stouthamer, E., & Addink, E. A. (2018). The relation between land use and subsidence in the Vietnamese Mekong delta. *Science of The Total Environment*, 634, 715–726.
- Tafreshi, G. M., Nakhaei, M., & Lak, R. (2019). Land subsidence risk assessment using GIS fuzzy logic spatial modeling in Varamin aquifer, Iran. *GeoJournal*, 23, 1–21.
- Momeni, M., Shafiee, A., Heidari, M., Jafari, M. K., & Mahdavi, M. R. (2012). Evaluation of soil collapse potential in regional scale. *Natural hazards*, 64(1), 459–479.
- Nadiri, A. A., Chitsazan, N., Tsai, F. T. C., & Moghaddam, A. A. (2014). Bayesian artificial intelligence model averaging for hydraulic conductivity estimation. *Journal of Hydrologic Engineering*, 19(3), 520–532.
- Nakhaei, M., Mohebbi Tafreshi, A., & Mohebbi Tafreshi, G. (2019). Modeling and predicting changes of TDS concentration in Varamin aquifer using GIS software. *Journal of Advanced Applied Geology*. <https://doi.org/10.22055/aag.2019.27539.1903>.
- Nejatjahromi, Z., Nassery, H. R., Hosono, T., Nakhaei, M., Alijani, F., & Okumura, A. (2019). Groundwater nitrate contamination in an area using urban wastewaters for agricultural irrigation under arid climate condition, southeast of Tehran, Iran. *Agricultural Water Management*, 221, 397–414.
- Pacheco, J., Arzate, J., Rojas, E., Arroyo, M., Yutsis, V., & Ochoa, G. (2006). Delimitation of ground failure zones due to land subsidence using gravity data and finite element modeling in the Querétaro valley, México. *Engineering Geology*, 84(3–4), 143–160.
- Paul, M. J. (2006). Impact of land-use patterns on distributed groundwater recharge and discharge. *Chinese Geographical Science*, 16(3), 229–235.
- Pérez, A. J., Hurtado-Patiño, J., Herrera, H. M., Carvajal, A. F., Pérez, M. L., Gonzalez-Rojas, E., et al. (2019). Assessing sub-regional water scarcity using the groundwater footprint. *Ecological Indicators*, 96, 32–39.
- Sheikhipour, B., Javadi, S., & Banihabib, M. E. (2018). A hybrid multiple criteria decision-making model for the sustainable management of aquifers. *Environmental Earth Sciences*, 77(19), 712.
- Szucs, P., Madarasz, T., & Civan, F. (2009). Remediating over-produced and contaminated aquifers by artificial recharge from surface waters. *Environmental Modeling and Assessment*, 14(4), 511–520.
- Valivand, F., & Katibeh, H. (2019). Application of numerical modeling and evaluate the effects of management scenarios in groundwater resources. *International Transaction Engineering Management Science Technology*. <https://doi.org/10.14456/ITJEMAST.2020.107>.
- World water assessment programme (United Nations), and UN-Water. (2009). *Water in a changing world*, 1. Earthscan.